A Nanotube-Supported Dicopper Complex Enhances Pt-free Molecular H-2/Air Fuel Cells

Solène Gentil, Jennifer K. Molloy, Marie Carrière, Ahmad Hobballah, Arnab Dutta, Serge Cosnier, Wendy J. Shaw, Gisèle Gellon, Catherine Belle, Vincent Artero, et al.

A Nanotube-Supported Dicopper Complex Enhances Pt-Free Molecular H_2/Air Fuel Cells

S. Gentil, [a,b] J. K. Molloy, [a] M. Carrière, [a] A. Hobballah [a] A. Dutta, [c] S. Cosnier,[a] W. J. Shaw, [c] G. Gellon, [a] C. Belle, [a] V. Artero,*[b] F. Thomas,*[a] and A. Le Goff*[a]

Affiliations

[a] Dr S. Gentil, Dr. J. K. Molloy, A. Hobballah, Dr S. Cosnier, G. Gellon, Dr C. Belle, Prof. F. Thomas, Dr A. Le Goff
Univ. Grenoble Alpes, CNRS, DCM, 38000 Grenoble, France
E-mail: alan.le-goff@univ-grenoble-alpes.fr, fabrice.thomas@univ-grenoble-alpes.fr,

[b] Dr S. Gentil, Dr V. Artero
Univ. Grenoble Alpes, CEA, CNRS, Laboratoire de Chimie et Biologie des Métaux, 38000 Grenoble, France
E-mail: vincent.artero@cea.fr

[c] Dr. W.J. Shaw and Dr. A. Dutta
Pacific Northwest National Laboratory, Richland, WA 99532, USA
E-mail: wendy.shaw@pnnl.gov

Dr. A. Dutta current address: Chemistry Department, IIT Gandhinagar, Gujarat 382355, India

Lead contact: alan.le-goff@univ-grenoble-alpes.fr

Summary: A dinuclear copper complex mimicking the active site of copper oxidases was designed and π-stacked on carbon-nanotube (CNT) electrode thanks to pendent pyrene groups. The high ORR activity of such CNT-supported dicopper complexes in pH 4 electrolyte allowed the construction of a Pt-free hydrogen/air fuel cell using bio-inspired nickel bisdiphosphine complexes immobilized onto CNT at the anode, with an order of magnitude improvement of the performance compared to previous literature data. This bio-inspired nickel- and copper-based H_2/air fuel cell reaches a maximum power density of 0.15 mW cm^{-2} at 0.25 V and pH 4.

Keywords: oxygen reduction • copper • carbon nanotubes • fuel cell • bioinspired catalyst

Introduction

Hydrogen fuel cells are a key technology for the ecological transition away from fossil fuels. They, however, rely on platinum-based catalysts used both at the anode and cathode to harvest electrical energy from hydrogen and air, respectively. The scarcity and high price of noble metals therefore impede the future deployment of hydrogen fuel cells unless efficient and stable catalysts based on Earth-abundant elements are found for the hydrogen oxidation (HOR) and oxygen reduction reactions (ORR).[1,2] Metalloenzymes hold promise in that context because they contain only first row transition metals at their active sites while approaching platinum like performances for both HOR and ORR.[3] Hydrogenases operate at the equilibrium potential of the $2H^+/H_2$ couple and display high HOR catalytic currents when immobilized on carbon-based electrodes.[4–6] Multicopper oxidases such as laccases have also shown efficient electrocatalytic performance towards ORR with low overpotential requirements.[7,8] The fact that sulfonated proton-exchange polymers are employed as solid electrolyte in conventional fuels, proton-exchange membrane fuel cells (PEMFCs), require that catalysts have be operational in a low-water-content medium and acidic environment. Unfortunately, metalloenzymes only operate in a narrow range of buffered conditions and few of them would withstand the conditions required for operation in PEMFC.

Bio-inspired catalysts have been developed for several years in order to reproduce enzymatic activity while allowing integration into conventional fuel cell systems.[9–15] These mimics reproduce both the structure of the enzyme active sites (first coordination sphere) and the electron/proton relays surrounding the active sites in the outer sphere. They now approach enzyme's low

overpotential requirements and high turnover frequencies. Namely, DuBois' mononuclear nickel *bis*-diphosphine $[Ni(P^R_2N^{R'}_2)_2]^{n+}$ complexes containing proton relays in the vicinity of the nickel center,[16–18] have been intensively investigated. The recently-developed $[Ni^{II}(P^{Cy}_2N^{Arg}_2)_2]^{7+}$ complex displays reversible $H_2/2H^+$ electrocatalytic behavior in acidic aqueous media.[19] We recently immobilized such Ni catalysts on carbon nanotubes (CNTs) and demonstrated their high efficiency towards HOR and their ability to operate in conventional PEMFC.[20–22]

Conversely, the design of highly efficient copper catalysts mimicking multicopper oxidases (MCOs) for ORR is not as mature as for hydrogenase models. Only few examples of dinuclear copper complexes have demonstrated ORR activity in the acidic environment required for implementation in PEMFCs.[23–28] Mononuclear Cu complexes also proved active for ORR in acidic conditions. In this regard, we have recently shown that a mononuclear copper complex based on the sterically hindered tripodal ligand **HMeBMP^{tBu}-pyrene** [29] mimicking galactose oxidase's active site, catalyzes ORR at onset potentials close to the enzymes.[30] Tyrosinase, bearing a *type 3* Cu_A-Cu_B active site, displays lower overpotential requirements towards ORR compared to galactose oxidase and catalyzes oxygen reduction in water at onset potentials of 0.60 V vs RHE (pH = 7).[31] To progress toward more efficient ORR catalysts, we therefore designed a bio-inspired dinuclear copper complex based on a HBPMP-type ligand functionalized with a pyrene moiety (Chart 1). These series of ligands were used previously to prepare μ-phenoxido dicopper(II) complexes, models of the active site of tyrosinase, initially studied in solution [32]. We then immobilized this complex at the surface of multi-walled CNT (MWCNT) electrodes due to π–π interactions between pyrene and CNT sidewalls, leading to novel copper-based nanostructured electrodes with ORR activity. These ORR cathodes were combined with a previously described bio-inspired anode material in order to design the first example of a bio-inspired nickel- and copper-based H_2/air fuel cell.

Results and discussion

The synthesis of the **HBPMP-pyrene** ligand is based on a peptidic coupling between 1-pyrenebutyric acid and the amino-functionalized ligand **HBPMP-NH$_2$** (see ESI). Subsequent reaction with 2 eq. of copper(II) salt affords the dicopper(II) complex **[Cu$_2$(BPMP-pyrene)]** (Fig. 1A). While the complex **[Cu$_2$(BPMP-pyrene)]** used for the preparation of functionalized MWCNT electrodes was synthetized 'in situ' from HBPMP-pyrene ligand and a copper salt, the complex was also isolated in the μOH form (see ESI for details).

In order to gain insight into the speciation of **[Cu$_2$(BPMP-pyrene)]**, we monitored pH titrations of *in situ* prepared complexes (pH_s range 2-7 in a H_2O:DMF 7:3 medium, or [DMF] concentration in water of 3.9 M, to ensure sufficient solubility of the complexes) with UV-Vis spectroscopy (Fig. S2 to S7).[33] We observed that **[Cu$_2$(BPMP-pyrene)]** exists under three distinct protonation states, which correspond to the phenolic "non bridged" form (low pH_s), a "bis(H_2O)" form, which predominates at pH_s around 4, and a "μOH" form at neutral pH_s (Scheme 1). The corresponding pKa values have been determined as 2.5±0.1 and 5.7±0.1 (Scheme 1). The structure assignment is based on both spectral similarities (Fig. S3-S8) and matching of pKa values with other BPMP-type binuclear complexes.[34,35]

The nature of the three species is also corroborated by EPR measurements (Fig. S9-S11): The "μOH" form is EPR-silent due to strong antiferromagnetic interactions between the Cu(II) centers through the two bridging ligands. The "bis(H_2O)" form shows spin triplet resonances, reminiscent of singly bridged **H-BPMP**-type dicopper complexes (Fig. 1B).[32,34] The zero field splitting (ZFS) parameter |D| obtained from simulation is 1500 MHz, corresponding to an intercopper distance of 4 Å [35] that nicely matches the value reported for structurally characterized H-BPMP-type dicopper complexes, wherein the exogenous ligand of each metal centre is a water molecule.[32,34,36] Even at pH=1.5 we did not observe free Cu(II) ion resonances, ruling out significant acid hydrolysis of the complex in the pH range investigated.

Multi-walled CNTs (MWCNTs) coated glassy-carbon electrodes were then functionalized with **[Cu$_2$(BPMP-pyrene)]** using two methods. The first one consists in generating *in situ* **[Cu$_2$(BPMP-pyrene)]** in a DMF/H_2O mixture (1:1 v/v) through addition of two equivalents of $[Cu(ClO_4)_2].6H_2O$ to a solution of **HBPMP-pyrene**. Next, MWCNT electrodes were soaked in this concentrated solution of **[Cu$_2$(BPMP-pyrene)]** for 1 hour**.** The second method is based on a two-step synthesis of the complex at the MWCNT surface. The first step consists of soaking a MWCNT electrode in a solution of **HBPMP-pyrene** to immobilize it at the surface of MWCNTs. Then a 0.3 M $[Cu(ClO_4)_2].6H_2O$ solution (in ultrapure water) was drop-cast onto the **HBPMP-pyrene**/MWCNT electrode (scheme 3). Both methods lead to electrodes functionalized by the dicopper complex, which exhibit similar electrochemical properties. It is noteworthy that no free Cu^{2+} ions have been detected at the surface of these MWCNT electrodes, either by CV or EPR experiments.

The functionalized MWCNT electrodes were characterized by X-ray photoelectron spectroscopy (Fig. S12) and cyclic voltammetry (CV) under Ar over a wide range of pH values (Fig. 2). The XPS analysis confirmed the presence of a Cu(II) complex at the surface of the electrode for both ligands, as indicated by the peaks at 934.8 and 954.2 eV, which are assigned to the Cu $2p_{1/2}$ and $2p_{3/2}$ binding energy, respectively. These features are accompanied by a typical weak satellite peak for Cu(II) at 944 eV. The low signal to noise ratio in the XPS data for the Cu(II) species is a consequence of Cu(II) reduction under the X-ray beam.[37]Furthermore, integration of the N 1s energy level, observed at 400 eV, and the Cu 2p gives an estimation of the ratio N/Cu of 2.7, closed to the theoretical ratio N/Cu of 7/2.

The electrochemical behavior of the **[Cu$_2$(BPMP-pyrene)]**/MWCNT electrode was first investigated by CV under an inert atmosphere and over a wide pH range (Fig. 2A). The **[Cu$_2$(BPMP-pyrene)]**/MWCNT electrodes display a partially-reversible redox system at $E_{1/2}$ = -0.09 V vs SHE at pH 4, assigned to the Cu(II/)Cu(I) redox couple. The linear dependence of both anodic and cathodic peak currents with the scan rate confirms that this redox system corresponds to a surface-immobilized redox species. In addition, the high ΔE_p value of 100 mV at slow scan rates suggests an electrochemically-induced structural rearrangement of the copper coordination sphere, similar to other surface-confined copper complexes.[29,38] The inset of Fig. 2A shows that the potential of the partially-reversible redox system decreases with increasing pH. This dependence is well modeled using eq. (1)[39,40]:

$$E_{1/2} = E_{1/2}(Cu^{II/I}{}_{acid}) + \frac{2.3RT}{nF} * \log(1 + \frac{[K_a\text{ox}]}{[H^+]}) \qquad (1),$$

where R is the gas constant, T the temperature, F the Faraday constant and n the number of electron involved in the redox system. K_a^{ox} is the proton dissociation constant for the oxidized form and $E_{1/2}(Cu^{II/I}{}_{acid})$ is the limiting value of $E_{1/2}$ at pH below p*K*a. A good fit of the data could be obtained using n = 2, giving access to an $E_{1/2}(Cu^{II/I}{}_{acid})$ of -0.08 ± 0.01 V and a p*K*a^{ox} of 4.3 ± 0.2 (R^2 = 0.99). The pK_a^{ox} value is close to the pK_a value of 5.7 obtained from spectroscopic titrations for the equilibrium between the "μOH" form and the "bis(H_2O)" form. The slight difference in pKa values accounts for the difference in medium between H_2O:DMF 7:3 and 0.1 M Britton Robinson buffer.

This model accounts for a $2e^-/1H^+$ redox system which supports the presence of a dinuclear Cu(II) species (bis(H_2O) form) immobilized at the electrode surface, singly deprotonated upon reduction of both Cu centers (to yield a bis-Cu(I) μ(OH) complex). On the reverse scan, this partially-reversible redox system is accompanied by a second oxidation process at a more positive potential (Fig. 2). This might arise from a conformational change induced by the formation of the protonated Cu(I)-Cu(I) species. The fact that this second oxidation process is related to a protonation process is supported by the increase of this second oxidation peak upon decreasing the pH. The EC nature if this redox process is also confirmed by the fact that integration of the charge under the reduction peak corresponds to the sum of integrated charges under both oxidation peaks. From the integration of the charge under the reduction peak, a surface coverage of 1.3 (+/-0.4) nmol cm^{-2} was estimated for the **[Cu_2(BPMP-pyrene)].** As a control experiment, we also modified MWCNT electrodes with pyrene modified with a [bis(2-pyridinylmethyl)amino]methyl ligand (**BPA-pyrene**). These functionalized MWCNT electrodes show negligible ability to stabilize a coordinated copper complex on MWCNT electrode on the contrary of the **BPMP-pyrene** ligand (Figure S13).

The ORR activity of MWCNT electrodes modified with the dinuclear copper species was then investigated by a combination of CV, Rotating-Disk Electrode (RDE) and Rotating-Ring-Disk Electrode (RRDE) voltammetry experiments in the presence of O_2. The electrocatalytic properties were studied over a wide range of pH values (Fig. 3 and S14) in order to unravel the ORR mechanism. The **[Cu_2(BPMP-pyrene)]**/MWCNT electrode exhibits ORR electroactivity (Fig.3A and B) with an onset potential of +0.33 V (pH 4) and 0.18 V (pH 9) vs. SHE. This corresponds to onset potentials of +0.57 V at pH 4 and 0.71 V vs. RHE at pH 9. While these complexes are still below the best copper-complex-based electrodes for ORR, which reach onset potentials of 1.05 V in 0.1 M KOH,[41] the electrodes compare well with the best immobilized dinuclear Cu models operating in acidic conditions and based on substituted phenanthrolines (0.7 V vs RHE at pH 5)[27,42], hexaazamacrocycles (0.67 V at pH 7),[43] the 3,5-diamino-1,2,4-triazole (0.73 V vs RHE at pH 7)[25] and tris(pyridin-2-ylmethyl)amine (0.65 V at pH 5),[24] which are active under acidic to neutral conditions. Nevertheless, this onset potential is still 300 mV less positive than the one measured for the dicopper active site of immobilized tyrosinase on MWCNT (E_{onset} = 1.0 V vs RHE at pH = 7).[31] As previously mentioned, the presence of an EC process involving a protonation step might induce the more positive value, by 300 mV, of the ORR onset potentials compared to the reduction of the complex under Ar. The onset potential decreases linearly with increasing pH for all complexes, with a slope of 32 mV per pH unit. This is consistent with a $2e^-/H^+$ limiting step for ORR electrocatalysis, as previously observed for other mono- or dinuclear copper complexes. This indicates a rate-determining step corresponding to the 2e-reduction of a coordinated O_2 complex to form a coordinated hydroperoxo specie, possibly through a Cu_2O_2 adduct.[26,28,29,38]. Above pH 8, increased maximum current densities were observed for **[Cu_2(BPMP-pyrene)]**/MWCNT electrode, reaching 9.8 (+/- 2) mA cm^{-2}. This confirmed that optimal ORR activity of this type of complex occurs in basic conditions. According to the dicopper complex surface coverage, maximum turnover frequencies (TOF) of 40 (+/-12) s^{-1} (pH 9) could be estimated for **[Cu_2(BPMP-pyrene)]**/MWCNT electrode. It is noteworthy that no decrease of the immobilized **[Cu_2(BPMP-pyrene)]** electroactivity under both Ar and O_2 was observed after multiple cycles over the course of one day. Furthermore, **[Cu_2(BPMP-pyrene)]**/MWCNT electrode exhibits higher electrocatalytic ORR performances in terms of current densities and onset potentials as compared to pristine MWCNTs (figure 3A and 3B) and MWCNT modified with **BPA-pyrene** ligand (figure S15A and S15B).

The formation of hydrogen peroxide as a side product is indicated by a Koutecky-Levich study performed by RDE measurements (Fig. S16) on the diffusion-controlled oxygen reduction electrocatalytic wave and by RDDE (Fig 3C and Fig S15). For RDE, after background subtraction to avoid any contribution of MWCNTs, an apparent number of electrons of 2.7 (+/-0.2) for **[Cu_2(BPMP-pyrene)]** was determined, indicative of competition between $4e^-/4H^+$ and $2e^-/2H^+$ ORR mechanisms (yielding H_2O and H_2O_2, respectively). It is noteworthy that this n value might be underestimated since MWCNT electrodes are far from planar electrodes, the latter being implied in the ideal case of Koutecky-Levich formalism.[44,45] In order to more accurately estimate the number of electrons involved in the ORR, the amount of H_2O_2 that forms during ORR was further quantified by RDDE measurements (Fig. 3C and Fig. S17). Low amounts of H_2O_2 of 6% were generated during ORR at **[Cu_2(BPMP-pyrene)]**/MWCNT electrode as compared to MWCNTs (48 %). Furthermore, CVs measured in the presence of 10 mM H_2O_2 (Fig. S18) show that the immobilized dinuclear complexes catalyze the reduction of H_2O_2 into H_2O with an onset potential similar to ORR. Despite the fact that n values can be difficult to accurately measure at nanostructured electrodes,[45,46] MWCNTs are poor electrocatalysts for H_2O_2 reduction in comparison with **[Cu_2(BPMP-pyrene)]**/MWCNT electrode. The excellent ORR performance of the immobilized dicopper complexes can therefore be ascribed to a $2e^-$+$2e^-$ mechanism. The fact that ORR performances are closed to those of previously-described mononuclear complex [29] might indicate that the formation of a dicopper oxygen-adduct intermediate is involved in both the mononuclear and dinuclear phenoxido complexes.

Having established its ORR activity, we integrated the **[Cu_2(BPMP-pyrene)]** complex into a noble metal-free bio-inspired fuel cell. First, the **[Cu_2(BPMP-pyrene)]** complex was immobilized on a MWCNT-coated gas-diffusion electrode (GDE). As an anode we used, a previously reported SWCNT-coated GDE functionalized with the bio-inspired $[Ni^{II}(P^{Cy}{}_2N^{Arg}{}_2)_2]^{7+}$ complex.[20] Such an anode material indeed proved excellent for

H_2 oxidation in conventional fuel cells using either Pt/C or the multicopper enzyme bilirubin oxidase at the cathode.[20]

Fig. 4A shows the schematic representation of the noble metal-free fuel cell setup. Both electrodes were separated by a 5 mm thick teflon chamber in which 0.1 M Britton-Robinson buffer at pH=4 was introduced. The fuel cell was operated at 25°C. Both the anode and the cathode were supplied with humidified streams of H_2 (atmospheric pressure) and air respectively. Fig. 4B displays the polarization and power curves, resulting from successive galvanostatic discharges. The fuel cell delivers a remarkable maximum power density of 0.15 mW cm^{-2} at 0.25 V and pH 4, accompanied with an open-circuit voltage (OCV) of 0.6 V. This unprecedented fuel cell based on molecular nickel and copper synthetic complexes as HOR and ORR catalysts is the first example of a fully-molecular noble metal-free fuel cell. Although not as efficient as biofuel cells based on immobilized MCOs, this new device outperforms previously-designed fuel cells integrating molecular catalysts. For comparison, fuel cell based on Ni-Ru catalysts delivers 11 µW cm^{-2} with an OCV of 0.3 V[11] and 25 µW cm^{-2} with an OCV of 0.42 V[10]. Another one, composed of $[Ni^{II}(P^{Ph}{}_2N^{CH2pyrene}{}_2)_2]$-based anode and cobalt-based cathode, delivers 23 µW cm^{-2} with an OCV of 0.74 V.[9] Thus, the original association of biomimetic Ni and Cu catalysts (mimics of hydrogenases and copper oxidases, respectively) allowed for an order of magnitude increase of the performance of such bio-inspired fuel-cells and appear as an efficient strategy for designing a new generation of Pt-free fuel cells with improved activity.

Conclusion

In summary, we report the immobilization of a novel (µ-phenoxido)-dicopper complex on MWCNT electrodes. This material catalyzes oxygen reduction with maximum onset potentials of 0.71 V vs RHE and TOF of 40 s^{-1} under alkaline conditions with partial $4H^+/4e^-$ mechanism and limited H_2O_2 production. By integrating such a molecular bio-inspired dicopper complex at a fuel cell cathode together with a molecular nickel complex at the anode, a first proof of concept for a H_2/air fuel cell based on non-precious-metals has been established, with significant improvement of the performances compared to the state of the art. The polarization curves show that the device's performances are mainly limited by the electrocatalytic ORR properties of the dicopper catalyst. Efforts in our groups will now focus on the optimization of bioinspired multi-copper ORR catalysts with the aim of approaching the performance of mixed biomimetic/enzymatic systems,[20] while retaining the advantages of chemical systems.

Acknowledgements

This work was supported by the Ministère de l'Environnement, de l'Energie et de la Mer and the Agence Nationale de la Recherche through the LabEx ARCANE programe (ANR-11-LABX-0003-01) and the Graduate School on Chemistry, Biology and Health of Univ Grenoble Alpes CBH-EUR-GS (ANR-17-EURE-0003). The authors acknowledge support from the plateforme de Chimie NanoBio ICMG FR 2607 (PCN-ICMG). WJS and AD acknowledge the Office of Science Early Career Research Program through the U.S. Department of Energy, Basic Energy Sciences. PNNL is operated by Battelle for the US DOE.

Author contributions

S.G., J.K.M., M.C., A.H., A.D. and G.G. conducted the experiments and analyzed datas. W. S., C.B., S.C., F.T., V.A. and A.L.G analyzed and discussed the results. F.T., V. A. and A.L.G designed the experiments and wrote the paper.

Declaration of Interests

The authors declare no competing interests.

References

1. Shao, M., Chang, Q., Dodelet, J.-P., and Chenitz, R. (2016). Recent Advances in Electrocatalysts for Oxygen Reduction Reaction. Chem. Rev. *116*, 3594–3657.

2. Jaouen, F., Proietti, E., Lefèvre, M., Chenitz, R., Dodelet, J.-P., Wu, G., Chung, H.T., Johnston, C.M., and Zelenay, P. (2010). Recent advances in non-precious metal catalysis for oxygen-reduction reaction in polymer electrolyte fuel cells. Energy Environ. Sci. *4*, 114–130.

3. Artero, V. (2017). Bioinspired catalytic materials for energy-relevant conversions. Nat. Energy *2*, 17131.

4. Cracknell, J.A., Vincent, K.A., and Armstrong, F.A. (2008). Enzymes as Working or Inspirational Electrocatalysts for Fuel Cells and Electrolysis. Chem. Rev. *108*, 2439–2461.

5. Lubitz, W., Ogata, H., Rüdiger, O., and Reijerse, E. (2014). Hydrogenases. Chem. Rev. *114*, 4081–4148.

6. de Poulpiquet, A., Ranava, D., Monsalve, K., Giudici-Orticoni, M.-T., and Lojou, E. (2014). Biohydrogen for a New Generation of H2/O2 Biofuel Cells: A Sustainable Energy Perspective. CHEMELECTROCHEM *1*, 1724–1750.

7. Le Goff, A., Holzinger, M., and Cosnier, S. (2015). Recent progress in oxygen-reducing laccase biocathodes for enzymatic biofuel cells. Cell. Mol. Life Sci. *72*, 941–952.

8. Mano, N., and de Poulpiquet, A. (2017). O2 Reduction in Enzymatic Biofuel Cells. Chem. Rev. *118*, 2392–2468.

9. Tran, P.D., Morozan, A., Archambault, S., Heidkamp, J., Chenevier, P., Dau, H., Fontecave, M., Martinent, A., Jousselme, B., and Artero, V. (2015). A noble metal-free proton-exchange membrane fuel cell based on bio-inspired molecular catalysts. Chem. Sci. *6*, 2050–2053.

10. Matsumoto, T., Kim, K., Nakai, H., Hibino, T., and Ogo, S. (2013). Organometallic Catalysts for Use in a Fuel Cell. ChemCatChem *5*, 1368–1373.

11. Matsumoto, T., Kim, K., and Ogo, S. (2011). Molecular Catalysis in a Fuel Cell. Angew. Chem. Int. Ed. *50*, 11202–11205.

12. Dey, S., Mondal, B., Chatterjee, S., Rana, A., Amanullah, S.K., and Dey, A. (2017). Molecular electrocatalysts for the oxygen reduction reaction. Nat. Rev. Chem. *1*, UNSP 0098.

13. Fukuzumi, S., Lee, Y.-M., and Nam, W. (2018). Immobilization of Molecular Catalysts for Enhanced Redox Catalysis. ChemCatChem *10*, 1686–1702.

14. Coutard, N., Kaeffer, N., and Artero, V. (2016). Molecular engineered nanomaterials for catalytic hydrogen evolution and oxidation. Chem. Commun. *52*, 13728–13748.

15. Jaouen, F., Jones, D., Coutard, N., Artero, V., Strasser, P., and Kucernak, A. (2018). Toward Platinum Group Metal-Free Catalysts for Hydrogen/Air Proton-Exchange Membrane Fuel Cells. Johnson Matthey Technology Review *62*, 231–255.

16. Wilson, A.D., Newell, R.H., McNevin, M.J., Muckerman, J.T., Rakowski DuBois, M., and DuBois, D.L. (2006). Hydrogen Oxidation and Production Using Nickel-Based Molecular Catalysts with Positioned Proton Relays. J. Am. Chem. Soc. *128*, 358–366.

17. Shaw, W.J., Helm, M.L., and DuBois, D.L. (2013). A modular, energy-based approach to the development of nickel containing molecular electrocatalysts for hydrogen production and oxidation. Biochim. Biophys. Acta-Bioenerg. *1827*, 1123–1139.

18. DuBois, D.L. (2014). Development of Molecular Electrocatalysts for Energy Storage. Inorg. Chem. *53*, 3935–3960.

19. Dutta, A., Roberts, J.A.S., and Shaw, W.J. (2014). Arginine-Containing Ligands Enhance H2 Oxidation Catalyst Performance. Angew. Chem. Int. Ed. *53*, 6487–6491.

20. Gentil, S., Lalaoui, N., Dutta, A., Nedellec, Y., Cosnier, S., Shaw, W.J., Artero, V., and Le Goff, A. (2017). Carbon-Nanotube-Supported Bio-Inspired Nickel Catalyst and Its Integration in Hybrid Hydrogen/Air Fuel Cells. Angew. Chem. Int. Ed. *56*, 1845–1849.

21. Le Goff, A., Artero, V., Jousselme, B., Tran, P.D., Guillet, N., Metaye, R., Fihri, A., Palacin, S., and Fontecave, M. (2009). From Hydrogenases to Noble Metal-Free Catalytic Nanomaterials for H2 Production and Uptake. Science *326*, 1384–1387.

22. Tran, P.D., Le Goff, A., Heidkamp, J., Jousselme, B., Guillet, N., Palacin, S., Dau, H., Fontecave, M., and Artero, V. (2011). Noncovalent Modification of Carbon Nanotubes with Pyrene-Functionalized Nickel Complexes: Carbon Monoxide Tolerant Catalysts for Hydrogen Evolution and Uptake. Angew. Chem.-Int. Edit. *50*, 1371–1374.

23. Brushett, F.R., Thorum, M.S., Lioutas, N.S., Naughton, M.S., Tornow, C., Jhong, H.-R. "Molly," Gewirth, A.A., and Kenis, P.J.A. (2010). A Carbon-Supported Copper Complex of 3,5-Diamino-1,2,4-triazole as a Cathode Catalyst for Alkaline Fuel Cell Applications. 12185–12187.

24. Thorseth, M.A., Letko, C.S., Rauchfuss, T.B., and Gewirth, A.A. (2011). Dioxygen and Hydrogen Peroxide Reduction with Hemocyanin Model Complexes. Inorg. Chem. *50*, 6158–6162.

25. Thorum, M.S., Yadav, J., and Gewirth, A.A. (2009). Oxygen Reduction Activity of a Copper Complex of 3,5-Diamino-1,2,4-triazole Supported on Carbon Black. Angew. Chem. Int. Ed. *48*, 165–167.

26. Thorseth, M.A., Tornow, C.E., Tse, E.C.M., and Gewirth, A.A. (2013). Cu complexes that catalyze the oxygen reduction reaction. Coordination Chemistry Reviews *257*, 130–139.

27. McCrory, C.C.L., Devadoss, A., Ottenwaelder, X., Lowe, R.D., Stack, T.D.P., and Chidsey, C.E.D. (2011). Electrocatalytic O2 Reduction by Covalently Immobilized Mononuclear Copper(I) Complexes: Evidence for a Binuclear Cu2O2 Intermediate. J. Am. Chem. Soc. *133*, 3696–3699.

28. Fukuzumi, S., Lee, Y.-M., and Nam, W. (2018). Mechanisms of Two-Electron versus Four-Electron Reduction of Dioxygen Catalyzed by Earth-Abundant Metal Complexes. ChemCatChem *10*, 9–28.

29. Gentil, S., Serre, D., Philouze, C., Holzinger, M., Thomas, F., and Le Goff, A. (2016). Electrocatalytic O2 Reduction at a Bio-inspired Mononuclear Copper Phenolato Complex Immobilized on a Carbon Nanotube Electrode. Angew. Chem. Int. Ed. *55*, 2517–2520.

30. Abad, J.M., Gass, M., Bleloch, A., and Schiffrin, D.J. (2009). Direct Electron Transfer to a Metalloenzyme Redox Center Coordinated to a Monolayer-Protected Cluster. J. Am. Chem. Soc. *131*, 10229–10236.

31. Reuillard, B., Le Goff, A., Agnès, C., Zebda, A., Holzinger, M., and Cosnier, S. (2012). Direct electron transfer between tyrosinase and multi-walled carbon nanotubes for bioelectrocatalytic oxygen reduction. Electrochemistry Communications, 19–22.

32. Torelli, S., Belle, C., Gautier-Luneau, I., Pierre, J.L., Saint-Aman, E., Latour, J.M., Le Pape, L., and Luneau, D. (2000). pH-Controlled Change of the Metal Coordination in a Dicopper(II) Complex of the Ligand H−BPMP: Crystal Structures, Magnetic Properties, and Catecholase Activity. Inorg. Chem. *39*, 3526–3536.

33. The compound described in reference 17 has been reinvestigated in the H2O:DMF 70:30 medium, see ESI.

34. Belle, C., Beguin, C., Gautier-Luneau, I., Hamman, S., Philouze, C., Pierre, J.L., Thomas, F., Torelli, S., Saint-Aman, E., and Bonin, M. (2002). Dicopper(II) Complexes of H-BPMP-Type Ligands: pH-Induced Changes of Redox, Spectroscopic (19F NMR Studies of Fluorinated Complexes), Structural Properties, and Catecholase Activities. Inorg. Chem. *41*, 479–491.

35. Srinivasan, R., Sougandi, I., Velavan, K., Venkatesan, R., Verghese, B., and Sambasiva Rao, P. (2004). Synthesis and characterization of [Cu2(L)2(OCOCH3)(OCH3)]ClO4 {L=2-[(4-methyl-pyridin-2-ylimino)-methyl]-phenol}: EPR and X-ray studies. Polyhedron *23*, 1115–1123.

36. Li, L., Murthy, N.N., Telser, J., Zakharov, L.N., Yap, G.P.A., Rheingold, A.L., Karlin, K.D., and Rokita, S.E. (2006). Targeted Guanine Oxidation by a Dinuclear Copper(II) Complex at Single Stranded/Double Stranded DNA Junctions. Inorg. Chem. *45*, 7144–7159.

37. Losev, A., Rostov, K., and Tyuliev, G. (1989). Electron beam induced reduction of CuO in the presence of a surface carbonaceous layer: an XPS/HREELS study. Surface Science *213*, 564–579.

38. Tse, E.C.M., Schilter, D., Gray, D.L., Rauchfuss, T.B., and Gewirth, A.A. (2014). Multicopper Models for the Laccase Active Site: Effect of Nuclearity on Electrocatalytic Oxygen Reduction. Inorg. Chem. *53*, 8505–8516.

39. Lalaoui, N., Le Goff, A., Holzinger, M., and Cosnier, S. (2015). Fully Oriented Bilirubin Oxidase on Porphyrin-Functionalized

Carbon Nanotube Electrodes for Electrocatalytic Oxygen Reduction. Chem. Eur. J. *21*, 16868–16873.

40. Sorrentino, I., Gentil, S., Nedellec, Y., Cosnier, S., Piscitelli, A., Giardina, P., and Le Goff, A. (2018). POXC Laccase from Pleurotus ostreatus: A High-Performance Multicopper Enzyme for Direct Oxygen Reduction Reaction Operating in a Proton-Exchange Membrane Fuel Cell. ChemElectroChem *5*, 1–6.

41. Wang, F.-F., Zhao, Y.-M., Wei, P.-J., Zhang, Q.-L., and Liu, J.-G. (2017). Efficient electrocatalytic O2 reduction at copper complexes grafted onto polyvinylimidazole coated carbon nanotubes. Chem. Commun. *53*, 1514–1517.

42. McCrory, C.C.L., Ottenwaelder, X., Stack, T.D.P., and Chidsey, C.E.D. (2007). Kinetic and Mechanistic Studies of the Electrocatalytic Reduction of O2 to H2O with Mononuclear Cu Complexes of Substituted 1,10-Phenanthrolines. J. Phys. Chem. A *111*, 12641–12650.

43. Slowinski, K., Kublik, Z., Bilewicz, R., and Pietraszkiewicz, M. (1994). Electrocatalysis of oxygen reduction by a copper(II) hexaazamacrocyclic complex. J. Chem. Soc., Chem. Commun., 1087–1088.

44. Masa, J., Batchelor-McAuley, C., Schuhmann, W., and Compton, R.G. (2013). Koutecky-Levich analysis applied to nanoparticle modified rotating disk electrodes: Electrocatalysis or misinterpretation. Nano Res. *7*, 71–78.

45. Zhou, R., Zheng, Y., Jaroniec, M., and Qiao, S.-Z. (2016). Determination of the Electron Transfer Number for the Oxygen Reduction Reaction: From Theory to Experiment. ACS Catal. *6*, 4720–4728.

46. Shin, D., Jeong, B., Choun, M., Ocon, J.D., and Lee, J. (2014). Diagnosis of the measurement inconsistencies of carbon-based electrocatalysts for the oxygen reduction reaction in alkaline media. RSC Adv. *5*, 1571–1580.

List of captions

Figure 1. (A) Representation of the "bis(H_2O)" form of **[Cu_2(BPMP-pyrene)]** predominating at pH 4.8 and (B) X-Band EPR spectrum of a 0.4 mM solution of **[Cu_2(BPMP-pyrene)]** in H_2O:DMF 70:30 (+0.1 M $NaClO_4$) at pH_s = 4.8. The inset shows a magnification of the ΔM_S = 2 region. The black line represents the experimental spectrum; the red line is a simulated spectrum by considering the following Spin Hamiltonian parameters: (S = 1), two equivalent copper nuclei with g_1 = 2.08, g_2 = 2.10 (with g-strain), g_3 = 2.18 and $A_{Cu,1} = A_{Cu,2}$ = 50 MHz, $A_{Cu,3}$ = 400 MHz. |D| = 1500 MHz, E = 450 MHz. Microwave Freq. 9.634659 GHz, power 20 mW, Mod. Amp. 0.4 mT, Mod. Freq. 100 KHz. T = 13 K.

Chart 1. Structure of the **HBPMP-pyrene** ligand.

Scheme 1. Protonation equilibria and distinct forms of **[Cu_2(BPMP-pyrene)]**. The corresponding pKa_s are given above the arrows.

Chart 2. Schematic representation of the **[Cu_2(BPMP-pyrene)]-**functionalized MWCNT electrode .

Figure 2. CVs of **[Cu_2(BPMP-pyrene)]** immobilized on the MWCNT electrode collected at pH 4, 7, 9 (0.1 M Britton Robinson buffer) under argon (ν= 10 mV s^{-1}) with (inset) corresponding experimental (□) and fitted (dashed line) evolution of the redox potential of the Cu(II)/Cu(I) redox couple as a function of the pH. The geometrical surface of the electrode (0.07 cm^{-2}) was used to calculate current densities.

Figure 3. (A, B) CVs of pristine MWCNT (a, black) and **[Cu_2(BPMP-pyrene)]/MWCNT** electrode (b, blue) under (dashed line) Ar and (straight line) O_2 (0.1 M Britton Robinson buffer, (A) pH 4, (B) pH 9, ν= 10 mV s^{-1}) **;** (C) Plot of the disk current *vs* disk potential and the plot of the ring current *vs* disk potential for Rotating Ring Disk Electrode measurements performed under O_2 at the (a) pristine MWCNT, and (b) **[Cu_2(BPMP-pyrene)]**/MWCNT electrodes using linear sweep voltammetry (ν = 10 mV s^{-1}, 1500 rpm, 0.1 M Britton-Robinson buffer pH = 5, no background subtraction)

Figure 4. (A) Schematic representation of the H_2/air bio-inspired fuel cell; (B) CV of **[Cu_2(BPMP-pyrene)] MWCNT-coated** GDE under argon (blue dashed line, curve a) and under a flow of air (blue, curve b) ; CV of **[$Ni^{II}(P^{Cy}{}_2N^{Arg}{}_2)_2$]$^{8+}$-MWCNT-coated** GDE under argon (red dashed line, curve c) and under a flow of H_2 (red, curve d) ; 0.1 M Britton-Robinson buffer pH = 4 , ν = 10 mV s^{-1}, 25°C; (C) Polarization and power curves for (straight line) **[Cu_2(BPMP-pyrene)]**/[$Ni^{II}(P^{Cy}{}_2N^{Arg}{}_2)_2$ and (dashed line) MWCNT/[$Ni^{II}(P^{Cy}{}_2N^{Arg}{}_2)_2$] (0.1 M Britton-Robinson buffer pH = 4, 25°C)

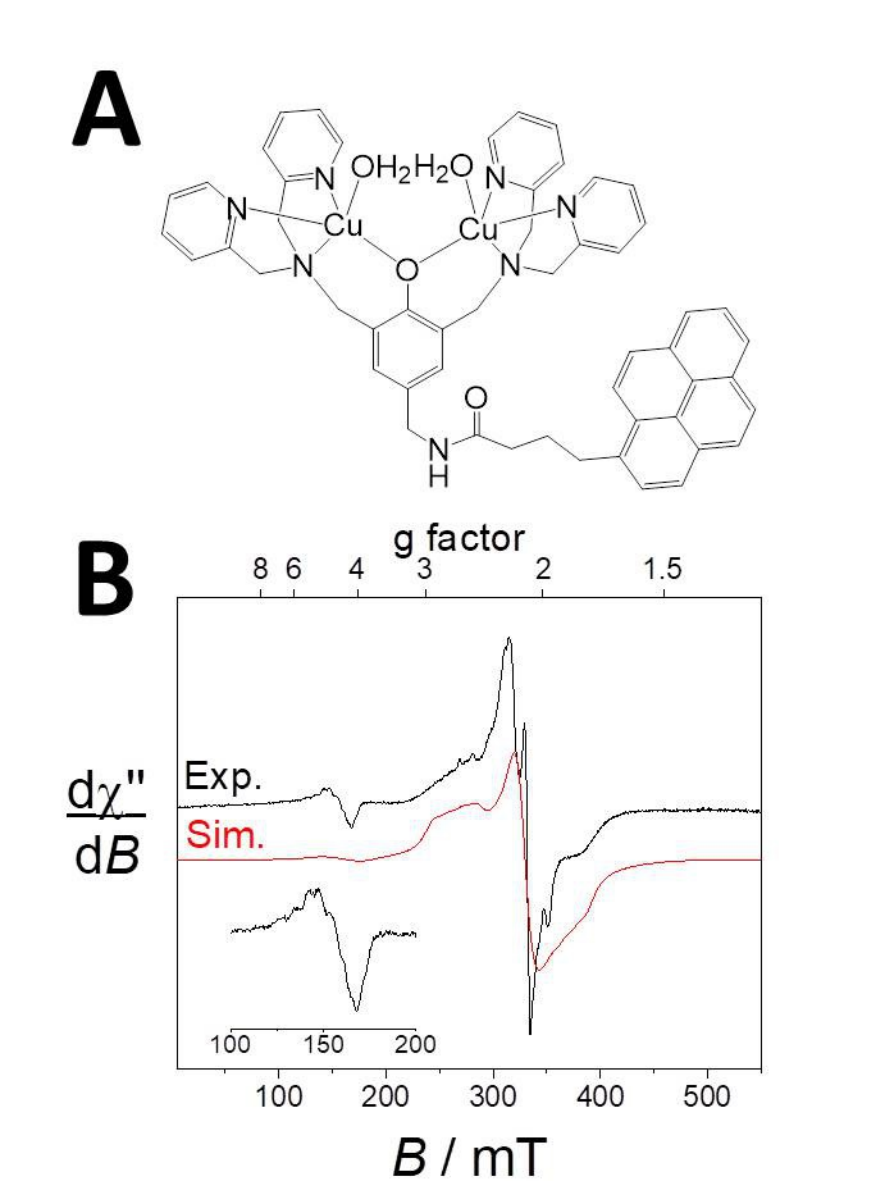
A
OH2H2O
N
Cu
Cu
O
N
H
B
g factor
8 6 4 3 2 1.5
dχ''
dB
Exp.
Sim.
100 150 200
100 200 300 400 500
B / mT

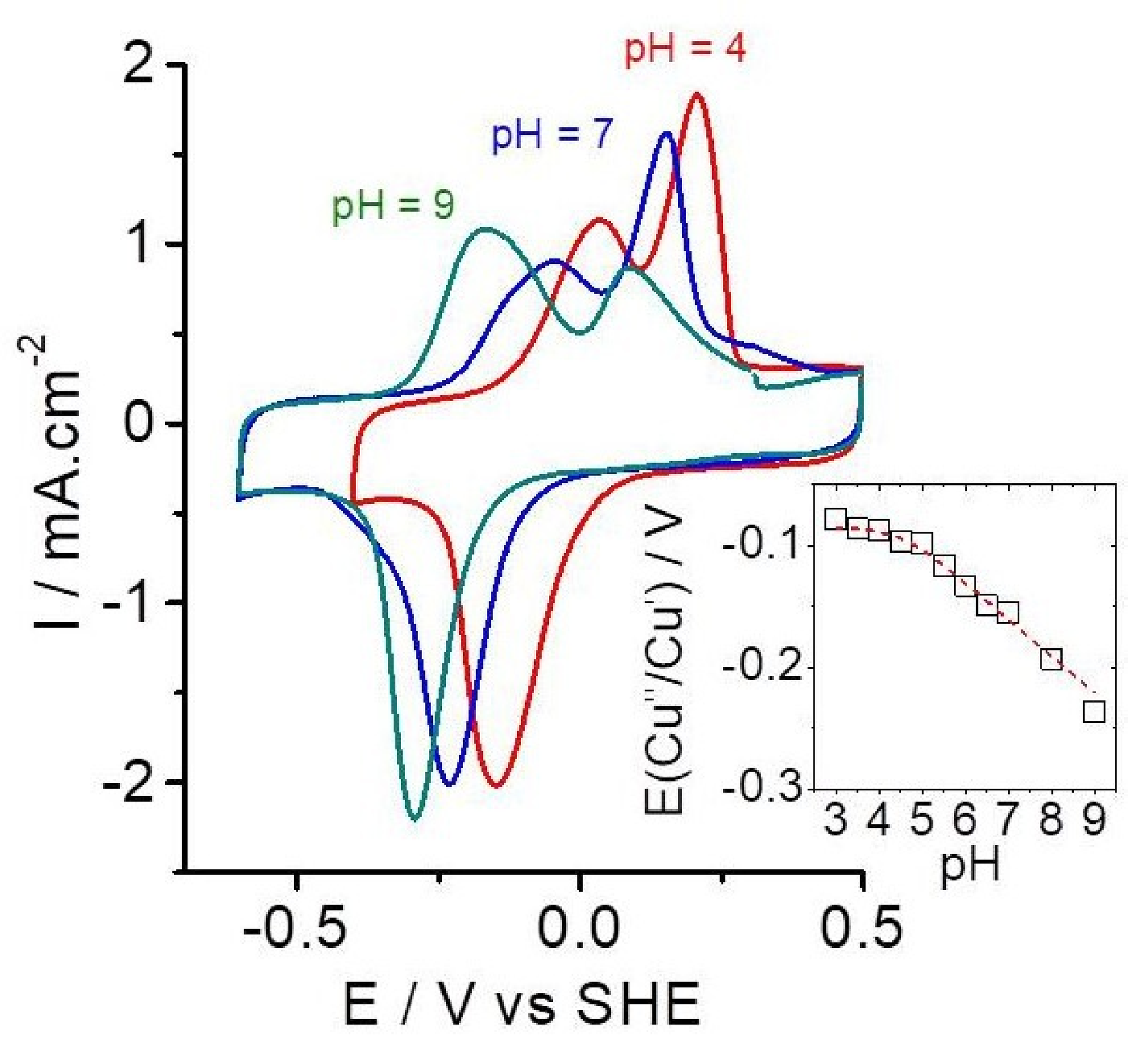
pH = 4
pH = 7
pH = 9
I / mA.cm-2
E / V vs SHE
E(Cu''/Cu') / V
pH

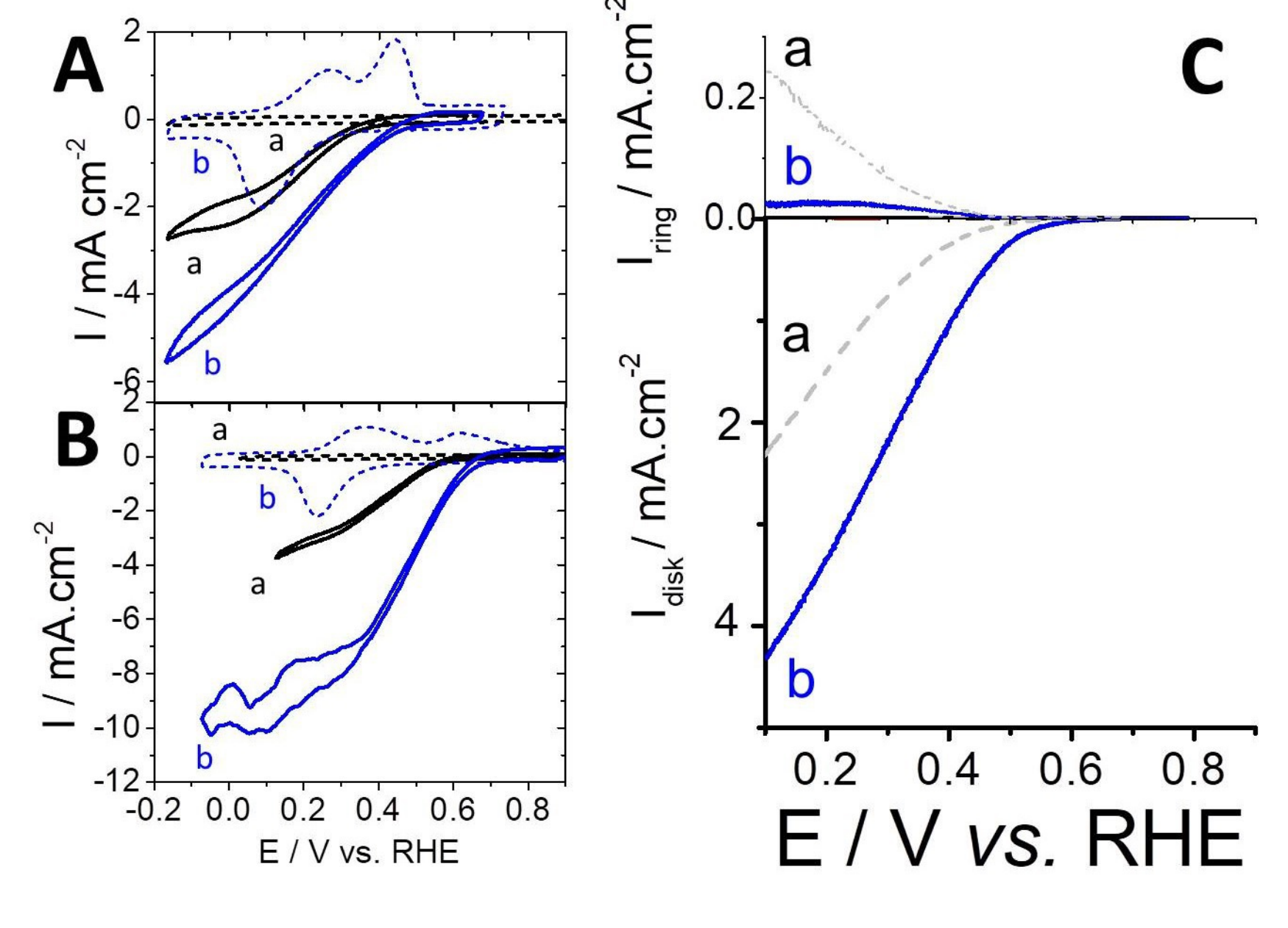
A
B
C
I / mA cm-2
I / mA.cm-2
E / V vs. RHE
a
b
I_ring / mA.cm-2
I_disk / mA.cm-2
E / V vs. RHE

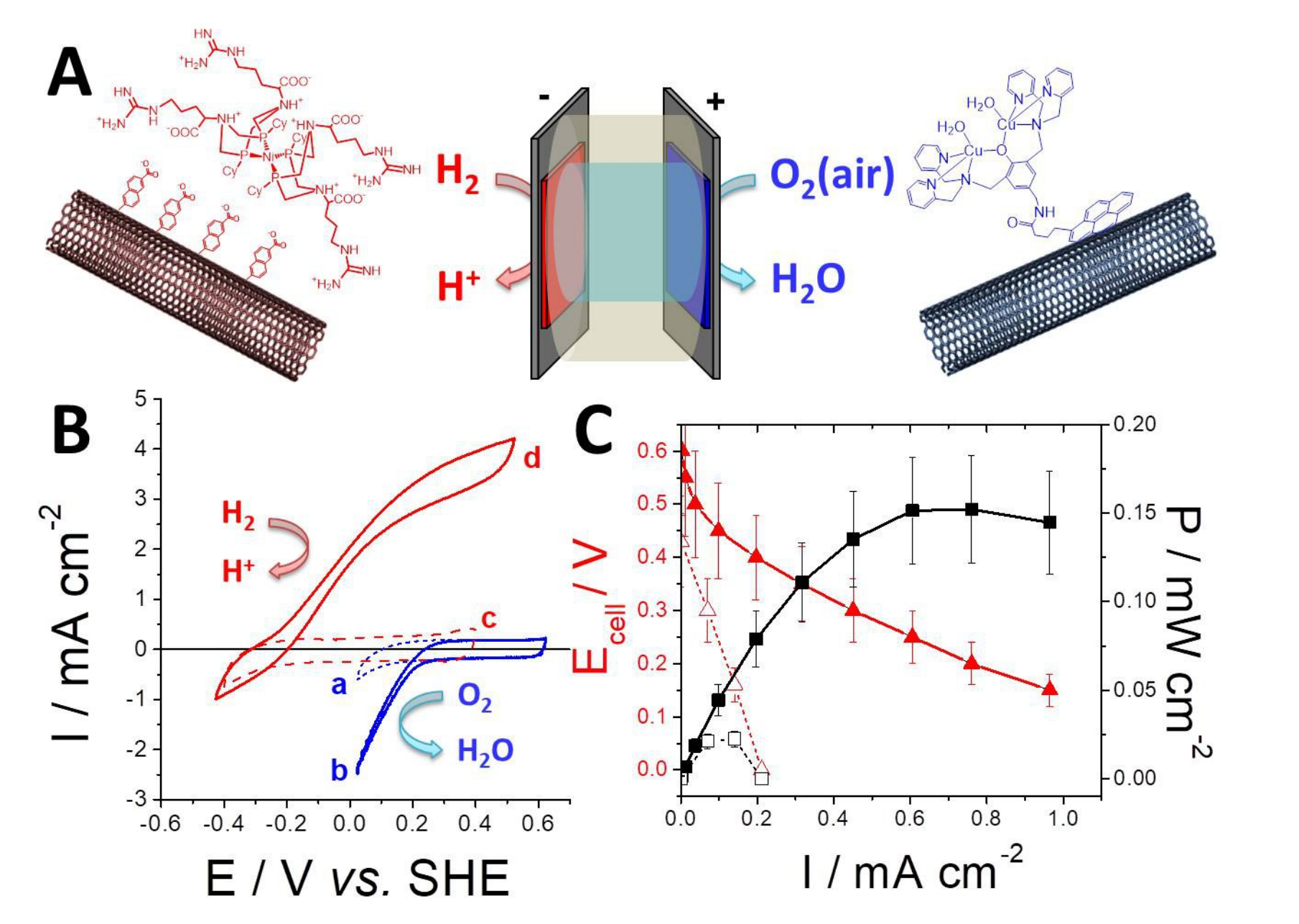
A
-
+
H2
H+
O2(air)
H2O
B
d
H2
H+
c
a
O2
H2O
b
I / mA cm-2
E / V vs. SHE
C
Ecell / V
P / mW cm-2
I / mA cm-2

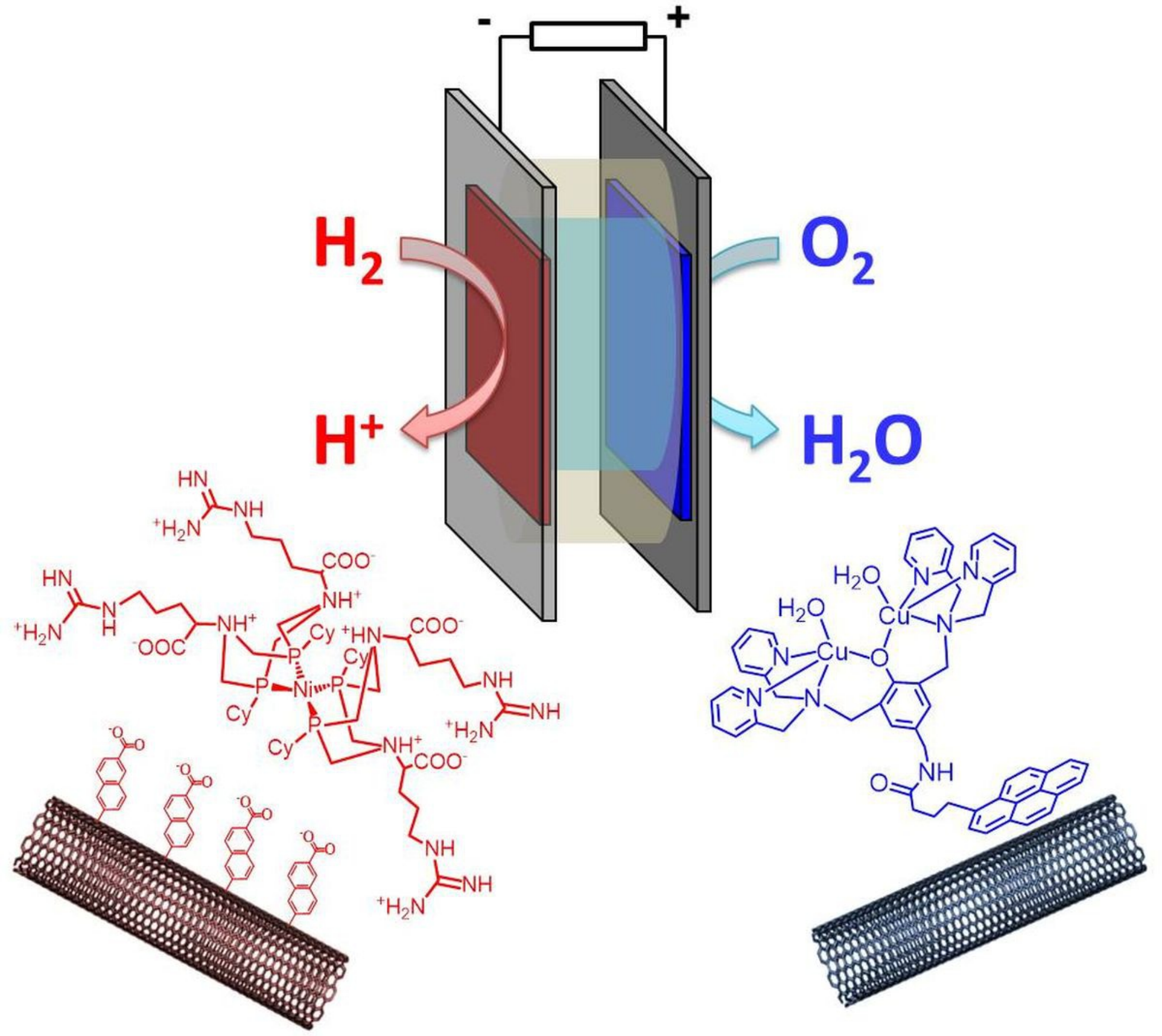
-
+
H2
O2
H+
H2O
HN
NH
+H2N
COO-
NH+
HN
N
H
+H2N
-OOC
NH+
Cy
+HN
COO-
P
Cy
P
Ni
P
Cy
NH
+H2N
NH
P
Cy
NH+
COO-
NH
+H2N
NH
-O
O
H2O
H2O
N
N
Cu
N
N
Cu
O
N
N
NH
O